8) *242-245 Remove the statement that the profile IS at steady state (here the authors rebut their own rebuttal). The comparison with rates elsewhere provides simply ZERO evidence that this system is at st st.*

There is no mention in the manuscript that the studied profile is at steady-state. This statement regards *soil-mantled hillslopes* in general , which has now been clarified in the revised text. Also, as indicated in the text, this interpretation is supported by other approaches (geomorphic transport laws and cosmogenic isotopes).

9) *Remove the entire section on erosion rates elsewhere, and delete the totally sloppy Fig 7. This discussion is mostly trivial (as stated in my first review Montgomeries rates are in part from highly land-used areas and hence not useful to compare with natural settings), and the fact that Alpine settings need to weather faster is most trivial, and in any case explaining one single rate (of which the significance as a "rate" is even disputable) does not justify a global comparison.*

As mentioned above, we believe that considering the high profile of the journal and its broad audience, a discussion about the broader implications of U-series isotope studies of weathering profiles is justified, as is the presence of Fig. 7 (now Fig. 8). We assert that putting our data in a global context and alongside similar data from a range of environmental settings provides a useful perspective. However, we agree that in the previous version, the figure was not as informative as it could be or should be. Upon revision, we have split up the U-series data into the different environmental settings rather than presented together in a single block. Finally, a careful study of the sources used in Montgomery's paper shows that few rates are derived from highly land-used areas and most of them come from natural settings and we have explained this in the figure caption.

Rapid regolith formation over volcanic bedrock and implications for landscape evolution

Anthony Dosseto[1,*], Heather L. Buss[2,+] and P.O Suresh[3]

[1] GeoQuEST Research Centre, School of Earth and Environmental Sciences, University of Wollongong. Wollongong, NSW, Australia
[2] USGS. Menlo Park, CA, USA
[3] Department of Physical Geography, Macquarie University. North Ryde, NSW, Australia
[+] now at School of Earth Sciences, University of Bristol. Bristol, UK.

*corresponding author: tonyd@uow.edu.au

Abstract

The ability to quantify how fast weathering profiles develop is crucial to assessing soil resource depletion and quantifying how landscapes evolve over millennia. Uranium-series isotopes can be used to determine the age of the weathering front throughout a profile and to infer estimates of regolith production rates, because the abundance of U-series isotopes in a weathering profile is a function of chemical weathering and time. This technique is applied to a weathering profile in Puerto Rico developed over a volcaniclastic bedrock. U-series isotope compositions are modelled, revealing that it takes 40-60 kyr to develop an 18m-thick profile. This is used to estimate an average regolith production rate of 334 ± 46 mm/kyr. This value is higher by a factor of up to 30 when compared to production rates estimated for weathering profiles developed over granitic or shale lithologies. This *quantitatively* underpins the lithological control on rates of regolith production (in a neighbouring watershed but over a granitic bedrock, production rates are only ~30-40 mm/kyr). Moreover, by comparing these results to a compilation of soil erosion rates, it is clear that landscapes are controlled by the balance (or imbalance) between regolith production and erosion: soil-mantled landscapes are the result of a relative balance between production and erosion, whereas in cratonic areas, thicker weathering profiles are generated because erosion fails to match regolith production rates.

Introduction

Quantifying the rate of conversion of bedrock into regolith through physical and chemical weathering is crucial for understanding landscape evolution over millennia and the coupling (or decoupling) between surface erosion at the top and bedrock weathering at the bottom of weathering profiles. The dynamics between these two interfaces dictate, at least partly, the evolution of soil resources, and more broadly of the *Critical Zone* (Brantley, 2008). Here we define *regolith* as the product of bedrock weathering as this term includes both the *saprolite* (the isovolumetric weathering product that retains the bedrock structure) and the overlying *soil* (the mobile uppermost layer of the weathering profile, produced from the saprolite by bioturbation, amongst other processes). In recent years, isotopic techniques have allowed us, for the first time, to quantify rates of regolith production. For instance, Heimsath et al. have used cosmogenic isotopes to show that soil production rates are inversely correlated to soil depth (Heimsath et al., 1997). To be able to discuss the evolution of soil resources, one needs to quantify soil erosion and production rates independently. However, the cosmogenic isotope technique requires assuming that these two rates are equal, suggesting that alternate approaches are needed to independently quantify rates of soil production. The measurement of uranium-series isotopes in erosion products can be used to determine the time elapsed since inception of bedrock weathering (Vigier et al., 2001; Dequincey et al., 2002; Vigier et al., 2005; Dosseto et al., 2006a; Dosseto et al., 2006b; Dosseto et al., 2006c; Vigier et al., 2006; Granet et al., 2007; Dosseto et al., 2008a; Dosseto et al., 2008b; Pelt et al., 2008; Dosseto et al., 2010; Granet et al., 2010; Ma et al., 2010). In a weathering profile, if one considers a sample at an elevation E, this timescale represents the amount of time elapsed between the time at which the bedrock-regolith interface was at elevation E and the present day (Fig.

1). Thus, this can be used to determine the age of the weathering front at different depths in a profile, termed throughout this manuscript the *weathering age* (Mathieu et al., 1995; Dequincey et al., 1999; Dequincey et al., 2002; Chabaux et al., 2003a; Chabaux et al., 2003b; Dosseto et al., 2008b; Pelt et al., 2008; Ma et al., 2010). Note that in previous studies this *weathering age* has been referred to as the *soil or saprolite residence time*. Regolith production rates can then be estimated either by considering the linear evolution of the weathering age with depth, when observed (as it is the case in this study), or by using the difference between the elevation of the regolith sample considered and the current elevation of the weathering front (Fig. 1). Note that neither approach requires any knowledge of the position, or the evolution, of the modern ground surface (like the surface lowering rate, for instance). Previous studies have focused on weathering profiles developed over granitic lithologies in different environments (tropical Brazil, Puerto Rico and Burkina-Faso, temperate Australia) and determined production rates ranging from about 10 to 70 mm/kyr (Mathieu et al., 1995; Dequincey et al., 2002; Dosseto et al., 2007; Dosseto et al., 2008b). More recently, a study of profiles underlain by shales has suggested similar rates (Ma et al., 2010). Here, we investigate regolith development over a volcaniclastic bedrock in Puerto Rico, as preliminarily presented in (Dosseto et al., 2011). The climate, topography, and vegetation at the study site is essentially the same as that of the neighbouring Rio Icacos catchment, where production and denudation rates have been obtained for profiles developed over quartz diorite using U-series and cosmogenic isotopes, respectively (Brown et al., 1995; Riebe et al., 2003; Blaes et al., under review). Thus, a comparison of these two neighbouring catchments provides an opportunity to assess the role of bedrock lithology, independent of climate, in controlling rates of soil production.

Study area

The studied weathering profile is located in the Bisley 1 catchment, the first of a series of 5 adjacent research catchments that feed into the Mameyes river basin, in the Luquillo Mountains of

45 eastern Puerto Rico (Fig. 2). This basin drains north to the Atlantic Ocean and is underlain by marine-
46 deposited basaltic to andesitic volcaniclastic bedrock with a history of hydrothermal alteration related to
47 the intrusion of the nearby quartz diorite stock. Relief in the 44 km² gaged area of the Mameyes
48 watershed is characterized by steep slopes with elevation varying between 80 and 1050 m. Elevation in
49 the Bisley watersheds ranges from 260-400 m. Mean annual temperature is 22 °C. Mean monthly
50 temperatures at the lowest elevations range from about 23.5 °C in January to 27 °C in September, and
51 from 17 °C to 20 °C at the highest elevations. Vegetation in the Mameyes watershed is mostly
52 subtropical to lower montane rainforest, with dwarf forests at the highest elevations and Sierra Palm
53 forests at lower elevations. The Bisley catchments are mostly covered by Tabonuco Forest. Precipitation
54 increases with elevation and ranges from 3000-4000 $mm.yr^{-1}$ (Scatena, 1990). The site was logged
55 extensively, but was reforested with native species in the 1950's (Scatena, 1989).
56 Cores (approximately 10 cm diameter) were taken through a weathering profile by hand-
57 augering to 15.7 m depth at site B1R (N18° 18.949, W65° 44.589), a 400 m elevation, ridge on the divide
58 between the Bisley 1 stream and a tributary of the Rio Sabana (Figure 2). The soils at the site are Ultisols
59 of the Humatas Series, which are 0.8-1.0 m deep, moderately well-drained, very-fine, parasesquic,
60 isohyperthermic Typic Haplohumults (Scatena, 1989; Silver et al., 1994; NCRS, 2002). Beneath the soil is
61 more than 15 m of saprolite: a soft, friable weathering product formed *in-situ* that retains the volume
62 and fabric of the parent bedrock. 33 soil and saprolite samples were collected from the auger, sieved to
63 2 mm, and analysed for mineralogy, major and trace elements (Supplementary Tables 1 and 2). Bedrock
64 was not reached during augering and the depth to bedrock is unknown but boreholes drilled near the
65 Bisley 1 stream gage encountered regolith to at least 37 m and a model of the bedrock-saprolite
66 interface based on the distribution of corestones in the watershed predicts that regolith on the
67 ridgetops could be as much as 135 m thick (Fletcher and Brantley, 2010; Buss et al., submitted).
68 Nevertheless, a bedrock sample was collected from a nearby outcrop that was exposed by a landslide at

approximately 350 m elevation; 50 m below the augering site on the slope of the same ridge. Although the composition of the parent rock varies across the catchment in terms of grain size and quartz content, this sample is consistent with the augered samples with respect to these parameters and is only used here as an estimate of the composition of the parent rock for comparison to the weathered samples. 11 out of 33 samples were analysed for U-series isotopes along with a bedrock sample. The scope of this article is restricted to discussing U-series isotope data, as mineralogical and other geochemical data will be discussed elsewhere.

Material and methods

Samples were homogenised and gently crushed in an agate mortar. About 30 mg of a solution enriched in ^{236}U-^{229}Th was added to ~100 mg of sample. This was then dissolved in a mixture of $HClO_4$, HF and HNO_3. Fluorides were driven off by evaporation at 100 °C and samples were then dried down by step evaporation at 150 °C, 170 °C and 200 °C. They were then taken up in 7M HNO_3 and loaded on a column containing AG1X8 anionic resin to separate U and Th. U and Th isotopes were measured on a Nu Instruments Nu Plasma multi-collector ICP-MS following procedures described in (Sims et al., 2008). Accuracy was checked by analysing gravimetric standard BCR-2. Four replicate analysis yield a ($^{234}U/^{238}U$) activity ratio = 0.991 ± 0.006 and ($^{230}Th/^{238}U$) = 0.999 ± 0.007 (parentheses denote activity ratios throughout this article). Replicate analysis was performed for a sample and used to determine relative external analytical uncertainties. These values are poor for U and Th concentrations, respectively 7.7 and 6.4 %, but as low as 0.2, 0.03 and 1.2% for ($^{234}U/^{238}U$), ($^{230}Th/^{238}U$) and ($^{230}Th/^{232}Th$) activity ratios, respectively. Poor external analytical uncertainty for U and Th concentrations could be explained by a heterogeneous distribution of these elements in the regolith. Note that this does not affect calculations and conclusions below, which are based on ($^{234}U/^{238}U$) and ($^{230}Th/^{238}U$) activity ratios only.

Results

The bedrock has U and Th concentrations of 0.75 and 1.04 ppm, respectively, which is generally lower than any values observed in the weathering profile (0.51-2.06 ppm and 1.43-2.67 ppm, respectively; Table 1). The ($^{234}U/^{238}U$) activity ratio in the bedrock is near secular equilibrium, whereas values greater than 1 are observed through the weathering profile (1.02-1.18). The ($^{230}Th/^{238}U$) in the bedrock is less than 1, and values in the weathering profile are all greater than 1 except for one sample (BIR370; sample depth = 370cm). Except for sample BIR370, both ($^{234}U/^{238}U$) and ($^{230}Th/^{238}U$) ratios increase with decreasing depth starting from near secular equilibrium at the bottom of the profile (Fig. 3). Note that there is evidence for sample BIR370 being less weathered compared to other samples: it has a CIA value of 89 (Table 1; Chemical Index of Alteration, CIA = (100)[$Al_2O_3/Al_2O_3 + CaO + Na_2O + K_2O$)]; (Nesbitt and Young, 1982)), compared to 97-99 in other samples (the weathering intensity increases with CIA values) (Supplementary Figure 1); it also has a WIP of 1390 (Weathering Index of Parker, WIP = (100)[($2Na_2O/0.35$) + ($MgO/0.9$) + ($2K_2O/0.25$) + ($CaO/0.7$)]; (Parker, 1970)) compared to 224-498 in other samples (the weathering intensity increases with decreasing WIP values). Except for this sample, CIA values (97-99) are greater than those determined at a weathering profile developed over granodiorite in the neighbouring Rio Icacos catchment (92-95; values calculated from (White et al., 1998)). ($^{230}Th/^{232}Th$) ratios show large variations, between 1.32 and 4.63, and the bedrock has a ($^{230}Th/^{232}Th$) within this range with a value of 1.75. ($^{230}Th/^{232}Th$) ratios increase with depth in the saprolite. Unlike ($^{234}U/^{238}U$) and ($^{230}Th/^{238}U$) ratios, ($^{230}Th/^{232}Th$) can be controlled by the abundance of different mineral phases with variable U/Th ratios and, as explained below, the ($^{230}Th/^{232}Th$) ratio in the saprolite is likely controlled by the abundance of goethite (probably characterized by a high U/Th ratio, inducing an increase in ($^{230}Th/^{232}Th$) values where this mineral is abundant).

Discussion

U-series isotope behaviour in bedrock and regolith

Higher U and Th concentrations in the weathering profile compared to the bedrock indicate that during regolith development these elements are relatively immobile compared to major soluble elements such as Na or Ca (e.g. (Brimhall and Dietrich, 1987)). Although the absence of significant ^{234}U-^{238}U disequilibrium in the bedrock would confirm that it has not undergone weathering, the presence of an excess of ^{238}U compared to ^{230}Th (i.e. (^{230}Th/^{238}U) <1) indicates either a recent loss of Th or a gain of U. This is surprising for two reasons: (i) if the rock is unweathered it should show secular equilibrium for this radioactive system too, especially considering that ^{230}Th-^{238}U reaches equilibrium before ^{234}U-^{238}U; (ii) water-rock interaction generally solubilises U over Th, leaving the residue enriched in Th over U, which is opposite to what is observed here. Because the rock was collected from an outcrop, it is possible that it has undergone enough interaction with meteoritic waters such that chemical weathering has disturbed the ^{230}Th-^{238}U equilibrium. Note that hydrothermal alteration cannot account for this disequilibrium as it took place more than 300 ka ago and any ^{230}Th-^{238}U disequilibrium incurred would have decayed back to secular equilibrium. Interestingly, basaltic weathering rinds studied by Pelt et al. (Pelt et al., 2008) show similar (^{230}Th/^{238}U) ratios (0.76-0.92). Thus, it is possible that the bedrock sample is showing the early stages of weathering rind development with a (^{234}U/^{238}U) near unity and a (^{230}Th/^{238}U) less than 1 (as observed in the weathering rind the closest to the interface with the fresh bedrock in (Pelt et al., 2008)). Although not discussed in Pelt et al., the (^{230}Th/^{238}U) ratio less than 1 is compatible with the hypothesis of a gain of U, which they invoked to explain U/Zr and (^{234}U/^{238}U) ratios.

^{234}U-^{238}U radioactive disequilibrium in solids is observed as a result of (i) recoil of ^{234}U into the surrounding medium (only measurable when the solid is fine-grained, typically silt size or smaller), (ii) preferential leaching of ^{234}U located in damaged sites of the crystalline network (Kigoshi, 1971; Fleischer,

136 1980, 1982; Hussain and Lal, 1986). Thus, the absence of ^{234}U-^{238}U disequilibrium in the bedrock sample,
137 combined with the observation of ^{230}Th-^{238}U disequilibrium, could suggest that preferential leaching of
138 ^{234}U over ^{238}U is not a significant process.

139 The continuous evolution of ($^{234}U/^{238}U$) and ($^{230}Th/^{238}U$) ratios in the weathering profile,
140 diagnostic of increasingly weathered and older regolith material with decreasing depth, contrasts with
141 the lack of systematic variation of weathering indexes such as CIA or WIP. The CIA is positively
142 correlated with Fe(III)-oxides and kaolinite and inversely correlated with quartz, reflecting precipitation
143 of secondary minerals and dissolution of quartz (Supplementary Table 1). Because the CIA and WIP
144 parameters do not have an inherent time constraint (i.e., radioactive decay) and are affected by multiple
145 geochemical and biogeochemical reactions, they are less robust proxies for weathering history than U-
146 series isotopes. For instance, Price and Velbel (2003) tested the various indices of weathering commonly
147 used by the community and concluded that CIA (along with other indices) is sensitive to other
148 geochemical processes in addition to weathering (e.g., hydrothermal alteration and other forms of
149 metamorphism). Moreover, an increase in CIA values with decreasing depth would be expected if CIA
150 solely recorded weathering. However, CIA values in the top half of the profile are lower than in the
151 bottom half. This could be explained by atmospheric input of Na, K and/or Ca, the precipitation of
152 secondary phases or by differential hydrothermal alteration histories of the protolith of the upper and
153 lower parts of the regolith profile.

154 U concentrations, U/Th and ($^{230}Th/^{232}Th$) ratios show a broad positive correlation with goethite
155 abundance (Fig. 4). Noting that the lowest U concentration is in the bedrock, this suggests that the
156 precipitation of goethite controls the abundance of uranium. Indeed, uranium is known to be strongly
157 sorbed to hydrous ferric oxides, such as goethite, in oxic systems at near-neutral pH (e.g., (Manceau et
158 al., 1992; Moyes et al., 2000; Giammar and Hering, 2001)) and sorption onto oxide and clay minerals has
159 been shown to control uranium concentrations in soils (e.g., (Gadelle et al., 2001)). Moreover, this

process seems to also control the ($^{230}Th/^{232}Th$) ratios in the regolith, where the range of observed values represents variable contributions between a "bedrock" end-member and a "goethite" end-member, the latter being characterized by a high ($^{230}Th/^{232}Th$) ratio. U concentrations and ($^{230}Th/^{232}Th$) ratios are also positively correlated with P_2O_5 concentrations (not shown), suggesting that the formation of a phosphorus-bearing phase could also partially control these geochemical parameters or reflecting adsorption of phosphate onto goethite. In contrast, ($^{234}U/^{238}U$) and ($^{230}Th/^{238}U$) ratios show no correlation with goethite content or any of the minerals quantified.

Timescale of regolith development

As the weathering front progresses downward into the bedrock, the extent of weathering should increase with decreasing depth in the weathering profile, and the time elapsed since production from the bedrock should increase with decreasing depth. Thus, since radioactive disequilibrium increases with time and extent of chemical weathering, an increase in disequilibrium with decreasing depth in the weathering profile is expected. Most previous work using U-series isotopes have focused on soils developed over granitic parent rock and this simple pattern of isotopic evolution was seldom observed (Mathieu et al., 1995; Dequincey et al., 1999; Dequincey et al., 2002; Chabaux et al., 2003a; Chabaux et al., 2008; Dosseto et al., 2008b). This is explained as weathering is not the only process occurring in soils but is accompanied by the complex transport of chemical elements and the precipitation and re-dissolution of secondary minerals. Nevertheless, here we observe that radioactive disequilibria for ^{234}U-^{238}U and ^{230}Th-^{238}U increases with decreasing depth (Fig. 3), similarly to what has been recently observed for soils developed over shales (Ma et al., 2007). The question why soils derived from granitic rocks would have a more complex U-Th history than those developed on clastic rocks is puzzling and should deserve more attention. Although a discussion of weathering in granitic environments is beyond the scope of this article, it is possible that the propagation of the weathering

front in this setting is not solely vertical but also lateral because of the presence of corestones, thus accounting for the complex U-Th patterns in granitic profiles.

In this section, we use the U-series isotope composition of the regolith to model the time elapsed since onset of weathering, i.e. the age of the weathering front, at different depths in the profile. In the model below, only ($^{234}U/^{238}U$) and ($^{230}Th/^{238}U$) are considered for the following reasons (Table 2): (i) unlike ($^{230}Th/^{232}Th$) or the Chemical Index of Alteration, ($^{234}U/^{238}U$) and ($^{230}Th/^{238}U$) are not affected by bedrock composition heterogeneity (including hydrothermal alteration, which has occurred here). This is because as long as the rock has been in a closed system for more than 1 Ma prior to weathering (which is the case here) ($^{234}U/^{238}U$) and ($^{230}Th/^{238}U$) =1, regardless of composition heterogeneities. (ii) ($^{234}U/^{238}U$) and ($^{230}Th/^{238}U$) are not affected by the selective dissolution of minerals. For instance, if we assume two minerals, A and B, with different U/Th ratios, where $U/Th_A > U/Th_B$. If mineral A is completely consumed during weathering, this will result in a relative decrease of U/Th and ($^{230}Th/^{232}Th$) ratios of the bulk material. Thus, the variation in ($^{230}Th/^{232}Th$) has no time information and cannot be used in the model. This is not the case for ($^{234}U/^{238}U$) and ($^{230}Th/^{238}U$): if mineral A is completely dissolved, any disequilibrium that was created during dissolution of mineral A is entirely transferred to the solution and the bulk material will have the isotopic composition of the residual minerals. Thus, ($^{234}U/^{238}U$) and ($^{230}Th/^{238}U$) ratios in the regolith are controlled by the isotopic composition of residual, U-bearing, actively dissolving minerals (e.g. micas, apatite if not completely dissolved; monazite is likely to be consumed early during weathering, whereas zircon are unlikely to dissolve in most cases). (iii) ($^{230}Th/^{232}Th$) correlates with goethite content suggesting that variations in this ratio are the result of the variable abundance of this mineral phase, unrelated to the duration of weathering. ($^{234}U/^{238}U$) and ($^{230}Th/^{238}U$) do not show any correlation with secondary mineral contents. Hence, note that the timescale calculated with these two ratios is not that of goethite formation. (iv) For extensively weathered profiles as it is the case here, common indices of weathering (like CIA) are of little use

because all soluble elements have been already mobilized. ($^{234}U/^{238}U$) and ($^{230}Th/^{238}U$) ratios do not have this limitation as they record weathering of residual mineral phases and U is less mobile than Ca, Mg, Na and K. Thus, these two isotopic ratios are valuable indices of weathering.

Dequincey et al. (2002) have proposed a model, later modified by Dosseto et al. (2008), to describe the evolution of nuclide abundance with time in regolith material:

$$\frac{dN_j}{dt} = \lambda_i.N_i - \lambda_j.N_j + f_j.N_{j,0} - k_j.N_j \quad (1)$$

where λ_i is the decay constant of the parent nuclide, N_i the abundance of the parent nuclide in the sample, λ_j the decay constant of the nuclide j, f_j an input coefficient for the nuclide j (in yr^{-1}), $N_{j,0}$ the initial nuclide abundance and k_j a dissolution coefficient for the nuclide j (in yr^{-1}). The input and dissolution coefficients are the time constants at which nuclide addition *via* chemical illuviation and/or dust input and removal *via* chemical weathering occur, respectively. These coefficients represent the different rates at which nuclide gain and loss operate. Using this model, the ($^{234}U/^{238}U$) and ($^{230}Th/^{238}U$) ratios in a regolith sample at a given depth are a function of the gain and loss coefficients for ^{238}U, ^{234}U and ^{230}Th, and the amount of time elapsed since onset of bedrock weathering, i.e. the age of the weathering front A_{wf}, at that depth (Fig. 1).

A major assumption of the model is that, although they take different values for each nuclide, they are assumed to be constant throughout the profile and over the age of the weathering front. A second major hypothesis is that nuclide gain (illuviation and/or dust input) occurs over a similar timescale to nuclide loss (chemical weathering). Although it is likely that these processes occur over different timescales, there are not enough constraints to allow nuclide loss and gain to operate over different timescales in the model presented. Another possible pitfall of the model is that the gain of nuclide does not differentiate between the precipitation of secondary mineral and dust input.

Nevertheless, dust input in the saprolite must be minimal (because of the nature of the saprolite, dust cannot be mechanically mixed with it) and secondary mineral precipitation must dominate.

The age of the weathering front, A_{wf}, will be different for each regolith sample, where A_{wf} is expected to increase with decreasing depth in the weathering profile. Thus, we look for the set of *k* and *f* coefficients for the weathering profile, and A_{wf} values for each sample that best reproduce the observed compositions. Considering the eleven samples analysed (including the replicate measurement of sample BIR687 to assess the sensitivity of the model to analytical error) and two activity ratios for each sample, ($^{234}U/^{238}U$) and ($^{230}Th/^{238}U$), we have 22 input parameters and 17 output parameters, or unknowns. We use a large-scale trust-region-reflective algorithm provided with the Matlab™ software to minimize the squared difference between calculated and observed activity ratios. This algorithm is a subspace-trust region method based on the interior-reflective Newton method described in (Coleman and Li, 1994, 1996). Because the solution could represent a local minimum, we generate a large population of solutions (n>100) from which the retained solution is the median of this population and the error on the calculated parameters (gain and loss coefficients and weathering ages) is the standard error of this population.

Results from the model are shown in Table 2. We considered different scenarios: model 1 uses the 11 samples measured and assumed secular equilibrium as initial conditions. Model 2 excludes BIR 370 as it is considered as an outlier on many aspects. Model 3 considers all the 11 samples measured but uses the measured composition of the bedrock sample as initial conditions. Results show that firstly, whether we consider as initial conditions a bedrock in secular equilibrium (i.e. before any water-rock interaction occurred; model 1) or the composition of the measured bedrock sample (model 3) this does not seem to significantly affect calculated weathering ages. Secondly, the model yields similar ages for replicate measurements of sample BIR687 (for instance, 26.8 and 27.2 kyr in model 1). Thirdly, calculated ages increase with decreasing depth, confirming the “ageing” of the regolith upward in the

254 weathering profile. Note that, when taking a weathering age equal to 0 for the bedrock, its ($^{234}U/^{238}U$)
255 ratio follows the correlation defined by soil samples, whereas its ($^{230}Th/^{238}U$) falls below (Suppl. Fig. 2). In
256 the latter case, this indicates that (i) either the unweathered bedrock shows an excess of U over Th and
257 chemical weathering follows a $1 - e^{-t/\tau}$ law where U is rapidly mobilized during the early stages of
258 weathering (τ being a characteristic timescale for weathering). This is unlikely as the bedrock is older
259 than 1 Myr and it should be in secular equilibrium for ^{230}Th-^{238}U; (ii) the bedrock is not representative of
260 the unweathered bedrock composition and this indicates that the early stage of bedrock weathering is
261 characterized by a loss of Th over U, or enrichment of U over Th. The latter hypothesis is supported by
262 the observation of similar ($^{230}Th/^{238}U$) ratios in our bedrock sample and in weathering rinds from a
263 basaltic corestone (Pelt et al., 2008).

264 Results from our calculations suggest that 40-60 kyr have elapsed since the weathering front
265 migrated from where the topsoil is today to its current position, i.e. a weathering age for the topsoil of
266 40-60 kyr (model 1, Fig. 5). Extrapolating the relationship between age and depth to 0 yr, the current
267 position of the weathering front can be estimated at a depth of ~ 16m, very close to the maximum
268 depth at which augering was possible. Moreover, the relative linear relationship between age and depth
269 (ruling out sample BIR370) suggests that the migration rate of the weathering front has been relatively
270 constant over the past 40-60 kyr. The regolith production rate, i.e. the migration rate of the weathering
271 front, can be determined as the slope in a weathering age versus depth space:

272 $$R = \frac{\Delta D}{\Delta A_{wf}} \quad (2)$$

273 where R is the regolith production rate (in mm/kyr) and D is depth (in mm). The age of the weathering
274 front, A_{wf}, is in thousands of years. In this case, the slope in Fig. 6 yields an average regolith production
275 rate of 334 ± 46 mm/kyr (error is 2σ). This value is greater than any production rate that has been
276 determined from U-series isotopes thus far (Fig. 7). Indeed, previous studies of weathering profiles

277 developed over granitic or shale substratum have yielded values between 10 and 70 mm/kyr. Thus, our
278 results could suggest that weathering profiles over volcaniclastic substratum are produced up to 30
279 times faster than in granitic regions. Note that this work is the first of its kind and further studies of
280 volcaniclastic weathering profiles need to be undertaken before this statement can be generalized.
281 Although it is well known that different lithologies weather at different rates, producing regolith more or
282 less rapidly, we are now able to *quantify* these differences. The geomorphic settings of the production
283 rates compiled in Fig. 8 vary: cratons in Brazil and Burkina-Faso (Mathieu et al., 1995; Dequincey et al.,
284 2002), soil-mantled hillslopes in Australia and eastern US (Dosseto et al., 2008b; Ma et al., 2010) and a
285 landslide-dominated landscape in Puerto Rico (this study and (Dosseto et al., 2007)). However, the range
286 of production rate values is narrow compared to that of soil erosion rates reported in (Montgomery,
287 2007) (Fig. 8). Thus, results from U-series studies suggest that, in general theweathering profile
288 thicknesses are in steady-state on soil-mantled hillslopes around the world (soil erosion ~ production) as
289 proposed earlier using geomorphic transport laws (Fernandes and Dietrich, 1997) or cosmogenic
290 isotopes (Heimsath et al., 1997) and previously verified using both U-series and cosmogenic isotopes at
291 a site in southeastern Australia (Dosseto et al., 2008b). Nevertheless, regolith production seems faster
292 than erosion on cratons, suggesting that weathering profiles in these regions are inexorably thickening.
293 In comparison, regolith production is not matched by erosion in alpine environments (Fig. 8), possibly
294 accounting for the bare rock landscape of these regions. However, studies need to be undertaken in
295 tectonically active environments in order to test this hypothesis. Finally, it is clear that, even in the light
296 of our results, natural rates of regolith production are too low compared to erosion rates in cultivated
297 areas. The quantitative determination of regolith production rates using U-series isotopes allows us to
298 estimate that regolith is lost 100 to 1,000 times faster than it is renewed in regions impacted by human
299 activity.

Conclusions

- A weathering profile developed over volcaniclastic bedrock under a tropical climate was studied with uranium-series isotopes to determine time constraints on soil formation in this environment.
- Bedrock collected from an outcrop show ^{230}Th-^{238}U disequilibrium similar to that observed in weathering rinds, but with ^{234}U-^{238}U in equilibrium indicating that (i) very early stages of water-rock interaction differentially mobilize chemical elements such as Th and U, and (ii) preferential leaching of ^{234}U over ^{238}U is not a significant process, at least for this lithology.
- Common indexes of chemical weathering (CIA, WIP) do not show any systematic variation through the profile. This is explained as they do not record the weathering of primary minerals solely, but also the formation of secondary phases and pre-weathering metamorphic alteration (U-series being insensitive to the latter, having occurred more than 1 Ma ago). In contrast, ^{238}U-^{234}U-^{230}Th radioactive disequilibria systematically increase with decreasing depth, as expected from an increasingly weathered profile from bottom to top.
- Modelling of U-series isotope composition in regolith indicates that it takes 40-60 kyr to produce 18m of weathering profile. The relationship between age of the weathering front and depth suggests that unweathered bedrock is located at ~16m depth and that the rate of migration of the weathering front (i.e. the regolith production rate) has been relatively constant over the past 40-60 kyr.
- A regolith production rate of 334 ± 46 mm/kyr is calculated. This is greater than any previously calculated rates for granitic and shale lithologies by a factor of 5 to 30. Although further studies of volcaniclastic weathering profiles need to verify such fast production rates, these results appear to underline the role of lithology on regolith formation rates, here *quantitatively* demonstrated. In particular, production rates of 30-50 mm/kyr were determined for a

weathering profile developed over quartz diorite in the neighbouring catchment of Rio Icacos, hence under similar climate (Blaes et al., under review).

- A compilation of U-series regolith production rates show that *steady-state weathering profile thickness is achieved in soil-mantled landscapes*. Nevertheless, in cratons, regolith production is faster than erosion and weathering profiles are thickening, whereas *in cultivated areas, regolith is lost 100 to 1,000 times faster than it is renewed*.

Acknowledgements

We would like to thank Sue Brantley, Arjun Heimsath, Lin Ma and Doug Burbank for useful discussions. We would also like to thank the editor, Gideon Henderson, and the reviewers (François Chabaux and two anonymous reviewers) for their comments which greatly improved the manuscript. Dosseto acknowledges an Australian Research Council (ARC) Future Fellowship FT0990447. Buss acknowledges support from the USGS Water Energy and Biogeochemical Budgets (WEBB) project and the NSF-Luquillo Critical Zone Observatory. Suresh acknowledges a Macquarie University Research Scholarship. This work was funded by an ARC Future Fellowship grant FT0990447 and an ARC Discovery grant DP1093708.

References

Blaes, E., et al., under review. U-series constraints for the rate of bedrock-saprolite transformation in the Rio Icacos watershed, Puerto Rico. Geochim. Cosmochim. Acta.

Brantley, S.L., 2008. Understanding Soil Time. Science 321, 1454-1455.

Brimhall, G.H., Dietrich, W.E., 1987. Constitutive mass balance relations between chemical composition, volume, density, porosity, and strain in metasomatic hydrochemical systems: Results on weathering and pedogenesis. Geochimica et Cosmochimica Acta 51, 567-587.

Brown, E.T., et al., 1995. Denudation rates determined from the accumulation of in-situ produced 10Be in the Luquillo Experimental Forest, Puerto Rico. Earth and Planetary Science Letters 129, 193-202.

Buss, H.L., et al., submitted. Probing the deep critical zone beneath the Luquillo Experimental Forest, Puerto Rico. Earth Surf. Proc. Landforms.

Chabaux, F., et al., 2008. U-Series Geochemistry in Weathering Profiles, River Waters and Lakes, Radioactivity in the Environment. Elsevier.

Chabaux, F., et al., 2003a. Tracing and dating recent chemical transfers in weathering profiles by trace-element geochemistry and 238U---234U---230Th disequilibria: the example of the Kaya lateritic toposequence (Burkina-Faso). Comptes Rendus Geosciences 335, 1219-1231.

Chabaux, F., et al., 2003b. U-Th-Ra fractionation during weathering and river transport, in: Bourdon, B., Henderson, G.M., Lundstrom, C.C., Turner, S.P. (Eds.), Uranium-series Geochemistry. Geochemical Society - Mineralogical Society of America, Washington, pp. 533-576.

Coleman, T.F., Li, Y., 1994. On the Convergence of Reflective Newton Methods for Large-Scale Nonlinear Minimization Subject to Bounds. Mathematical Programming 67, 189-224.

Coleman, T.F., Li, Y., 1996. An Interior, Trust Region Approach for Nonlinear Minimization Subject to Bounds. SIAM Journal on Optimization 6, 418–445.

Dequincey, O., et al., 1999. Dating of weathering profiles by radioactive disequilibria: Contribution of the study of authigenic mineral fractions. Comptes Rendus de l'Academie des Sciences - Series IIA - Earth and Planetary Science 328, 679-685.

Dequincey, O., et al., 2002. Chemical mobilizations in laterites: Evidence from trace elements and ^{238}U-^{234}U-^{230}Th disequilibria. Geochim. Cosmochim. Acta 66, 1197-1210.

Dosseto, A., et al., 2006a. Timescale and conditions of chemical weathering under tropical climate: Study of the Amazon basin with U-series. Geochim. Cosmochim. Acta 70, 71-89.
Dosseto, A., et al., 2006b. Weathering and transport of sediments in the Bolivian Andes: time constraints from uranium-series isotopes. Earth and Planetary Science Letters 248, 759-771.
Dosseto, A., et al., 2008a. Uranium-series isotopes in river materials: Insights into the timescales of erosion and sediment transport. Earth and Planetary Science Letters 265, 1-17.
Dosseto, A., et al., 2011. The delicate balance between soil production and erosion, and its role on landscape evolution. Applied Geochemistry 26, S24-S27.
Dosseto, A., et al., 2010. Climatic and vegetation control on sediment dynamics. Geology 38, 395-398.
Dosseto, A., et al., 2007. The timescale of sediment transport in a small tropical watershed. Geochim. Cosmochim. Acta 71, Suppl. 1.
Dosseto, A., et al., 2006c. Uranium-series isotopes in colloids and suspended sediments: timescale for sediment production and transport in the Murray-Darling River system. Earth Planet. Sci. Lett. 246, 418-431.
Dosseto, A., et al., 2008b. The evolution of weathering profiles through time: New insights from uranium-series isotopes. Earth and Planetary Science Letters 274, 359-371.
Fernandes, N.F., Dietrich, W.E., 1997. Hillslope evolution by diffusive processes: The timescale for equilibrium adjustments. Water Resour. Res. 33, 1307-1318.
Fleischer, R.L., 1980. Isotopic disequilibrium of uranium: Alpha-recoil damage and preferential solution effects. Science 207, 979-981.
Fleischer, R.L., 1982. Alpha-recoil damage and solution effects in minerals: uranium isotopic disequilibrium and radon release. Geochimica et Cosmochimica Acta 46, 2191-2201.
Fletcher, R.C., Brantley, S.L., 2010. Reduction of bedrock blocks as corestones in the weathering profile: Observations and model. American Journal of Science 310, 131-164.
Gadelle, F., et al., 2001. Removal of Uranium(VI) from Contaminated Sediments by Surfactants. J. Environ. Qual. 30, 470-478.
Giammar, D.E., Hering, J.G., 2001. Time scales for sorption-desorption and surface precipitation of uranyl on goethite. Environ. Sci. Technol. 35, 3332-3337.

Granet, M., et al., 2010. U-series disequilibria in suspended river sediments and implication for sediment transfer time in alluvial plains: The case of the Himalayan rivers. Geochim. Cosmochim. Acta 74, 2851-2865.
Granet, M., et al., 2007. Time-scales of sedimentary transfer and weathering processes from U-series nuclides: Clues from the Himalayan rivers. Earth and Planetary Science Letters 261, 389-406.
Heimsath, A.M., et al., 1997. The soil production function and landscape equilibrium. Nature 388, 358-361.
Hussain, N., Lal, D., 1986. Preferential solution of234U from recoil tracks and234U/238U radioactive disequilibrium in natural waters. Proceedings of the Indian Academy of Sciences - Earth and Planetary Sciences 95, 245-263.
Kigoshi, K., 1971. Alpha-recoil thorium-234: Dissolution into water and the uranium-234/uranium-238 disequilibrium in nature. Science 173, 47-48.
Ma, J.-L., et al., 2007. Mobilization and re-distribution of major and trace elements during extreme weathering of basalt in Hainan Island, South China. Geochimica et Cosmochimica Acta 71, 3223-3237.
Ma, L., et al., 2010. Regolith production rates calculated with uranium-series isotopes at Susquehanna/Shale Hills Critical Zone Observatory. Earth and Planetary Science Letters 297, 211-255.
Manceau, A., et al., 1992. Sorption and speciation of heavy metals on hydrous Fe and Mn oxides. From microscopic to macroscopic. Applied Clay Science 7, 201-223.
Mathieu, D., et al., 1995. Short-lived U and Th isotope distribution in a tropical laterite derived from granite (Pitinga river basin, Amazonia, Brazil): Application to assessment of weathering rate. Earth Planet. Sci. Lett. 136, 703-714.
Montgomery, D.R., 2007. Soil erosion and agricultural sustainability. Proceedings of the National Academy of Sciences of the United States of America 104, 13268-13272.
Moyes, L.N., et al., 2000. Uranium Uptake from Aqueous Solution by Interaction with Goethite, Lepidocrocite, Muscovite, and Mackinawite: An X-ray Absorption Spectroscopy Study. Environmental Science & Technology 34, 1062-1068.
NCRS, U., 2002. Soil Survey of Caribbean National Forest and Luquillo Experimental Forest, Commonwealth of Puerto Rico. USDA, Natural Resources Conservation Service, Washington, D.C.
Nesbitt, H.W., Young, G.M., 1982. Early Proterozoic climates and plate motions inferred from major element chemistry of lutites. Nature 299, 715-717.

Parker, A., 1970. An index of weathering for silicate rocks. Geological Magazine 107, 501-504.
Pelt, E., et al., 2008. Uranium-thorium chronometry of weathering rinds: Rock alteration rate and paleo-isotopic record of weathering fluids. Earth and Planetary Science Letters 276, 98-105.
Price, J.R., Velbel, M.A., 2003. Chemical weathering indices applied to weathering profiles developed on heterogeneous felsic metamorphic parent rocks. Chem. Geol. 202, 397-416.
Riebe, C.S., et al., 2003. Long-term rates of chemical weathering and physical erosion from cosmogenic nuclides and geochemical mass balance. Geochim. Cosmochim. Acta 67, 4411-4427.
Scatena, F.N., 1989. An introduction to the physiography and history of the Bisley Experimental Watersheds in the Luquillo Mountains of Puerto Rico, in: Service, U.F. (Ed.), General Technical Report, p. 22.
Scatena, F.N., 1990. Watershed scale rainfall interception on two forested watersheds in the Luquillo Mountains of Puerto Rico. Journal of Hydrology 113, 89-102.
Silver, W.L., et al., 1994. Nutrient availability in a montane wet tropical forest: Spatial patterns and methodological considerations. Plant and Soil 164, 129-145.
Sims, K.W.W., et al., 2008. An Inter-Laboratory Assessment of the Thorium Isotopic Composition of Synthetic and Rock Reference Materials. Geostandards and Geoanalytical Research 32, 65-91.
Vigier, N., et al., 2005. Mobility of U-series nuclides during basalt weathering: An example of the Deccan Traps (India). Chem. Geol. 219, 69-91.
Vigier, N., et al., 2001. Erosion timescales derived from U-decay series measurements in rivers. Earth Planet. Sci. Lett. 193, 546-563.
Vigier, N., et al., 2006. The relationship between riverine U-series disequilibria and erosion rates in a basaltic terrain. Earth and Planetary Science Letters 249, 258-273.
White, A.F., et al., 1998. Chemical weathering in a tropical watershed, Luquillo Mountains, Puerto Rico: I. Long-term versus short-term weathering fluxes. Geochim. Cosmochim. Acta 62, 209-226.

Figure legends

Figure 1. Illustration of the concept of age of the weathering front, termed *weathering age*, for two samples, A and B, in a profile. The weathering age for sample A, $A_{wf,A}$, represents the time elapsed between T_1, the time at which the bedrock-regolith interface was at elevation E_A and T_{now}, the present day: $A_{wf,a} = T_{now} - T_1$. The average regolith production rate over the distance E_AE_i, where E_i is the current elevation of the bedrock-regolith interface, can be estimated simply as $(E_A - E_i)/ A_{wf,A}$. Alternatively, if the weathering age increases linearly with decreasing depth (as it is the case in this study), the average regolith production rates over the entire profile can be calculated from the slope of age as a function of depth. Note that these approaches do not require any assumption on the steady-state nature of the profile thickness or knowledge of the denudation rate. This is illustrated in this example where erosion is taken to be nil (the same concepts would apply to actively eroding landscapes).

Figure 2. Simplified geological map of the Luquillo Critical Zone Observatory showing locations of the Bisley (B1R) and Icacos (LG1; e.g. (White et al., 1998)) weathering profiles in the Rio Mameyes and Rio Blanco catchments, respectively. Modified from http://www.sas.upenn.edu/lczo/mameyes.html.

Figure 3. ($^{234}U/^{238}U$) and ($^{230}Th/^{238}U$) activity ratios in soil versus depth. Sample BIR370 (depth = 370 cm) is relatively unweathered material (possibly a corestone) as evidenced by a low Chemical Index of Alteration and high K_2O and MgO content compared to other samples. This would explain why it shows radioactive disequilibrium very different from neighbouring samples.

Figure 4. Goethite abundance (in %) as a function of U concentrations (in ppm) and ($^{230}Th/^{232}Th$) ratios.

Figure 5. ($^{230}Th/^{238}U$) as a function of ($^{234}U/^{238}U$) activity ratios. Diamonds are data from the Bisley weathering profile and the curve is best-fit calculated with the inverse model described in the text (model 1 in Table 2). The curve is labelled with the weathering age in 1,000 years.

Figure 6. Calculated weathering age (in 1,000 years; model 1 in Table 2) as a function of depth (in cm).

Figure 7. Comparison of regolith production rates derived from U-series isotopes in various settings (range of values is shown; the x-axis shows the bedrock lithology). Regolith production over granitic rocks is relatively insensitive to climate. Whilst shales and granitic rocks apparently produce regolith at similar rates, the results from our weathering profile could suggest that volcanoclastic sedimentary lithologies produce regolith much faster. For same climatic conditions (compare with granodiorite lithology in Puerto Rico), regolith is produced 3 times faster over the volcanoclastic sedimentary rock than over granodiorite.

Figure 8. Soil/regolith production rates inferred from U-series isotopes compared to soil erosion rates in various settings (as termed in (Montgomery, 2007)). Ranges in values for erosion rates are taken from (Montgomery, 2007) and refs therein. Note that only rates next to the label “agriculture” are for land-used areas, all other rates are from natural environments. Soil/regolith production rates are from U-series studies in Fig. 7. The narrow range in production rates is likely to result from the limited number of U-series studies published thus far. Production rate estimates from Puerto Rico are shown as stars (left: Icacos site underlain by a quartz diorite, (Dosseto et al., 2007; Blaes et al., under review); right:

Bisley site, this study). In this figure, Puerto Rico is placed between soil-mantled landscapes and alpine regions because erosion is landslide-dominated, but it is not an actively uplifting area.

Supplementary Figue 1. Chemical Index of Alteration (CIA) as a function of depth. Sample BIR370 clearly shows that it is less weathered than other samples.

Supplementary Figure 2. ($^{234}U/^{238}U$) and ($^{230}Th/^{238}U$) activity ratios versus calculated weathering ages. Diamonds: soil, square: bedrock. As the age of the weathering front increases in the profile, ^{234}U is preferentially enriched over ^{238}U, as a possible result of addition of ^{234}U during precipitation of secondary phases, and ^{230}Th is enriched over ^{238}U, as uranium is more readily mobilized compared to thorium during chemical weathering.

Highlights

- A weathering profile developed over volcanoclastic bedrock under a tropical climate was studied with uranium-series isotopes.
- Modelling of U-series isotope composition in regolith indicates that it takes 40-60 kyr to produce 18m of weathering profile.
- A regolith production rate of 334 ± 46 mm/kyr is calculated. This is greater than rates for granitic and shale lithologies.
- A compilation of U-series regolith production rates show that *steady-state weathering profile thickness is achieved in soil-mantled landscapes*.

Figure 1

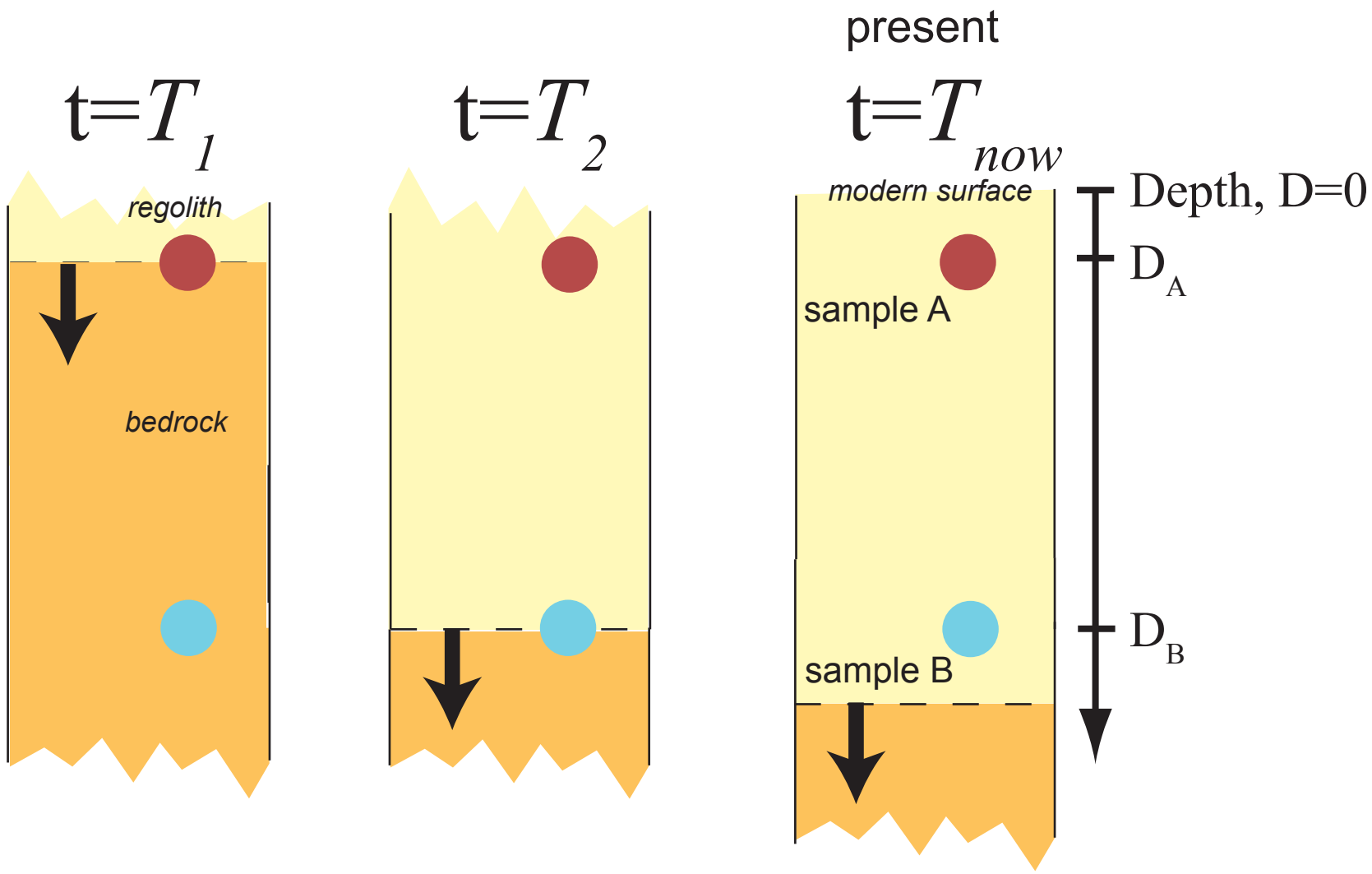

$$A_{wf,A} = T_{now} - T_1$$
$$A_{wf,B} = T_{now} - T_2$$
$$A_{wf,A} > A_{wf,B}$$

Figure 2

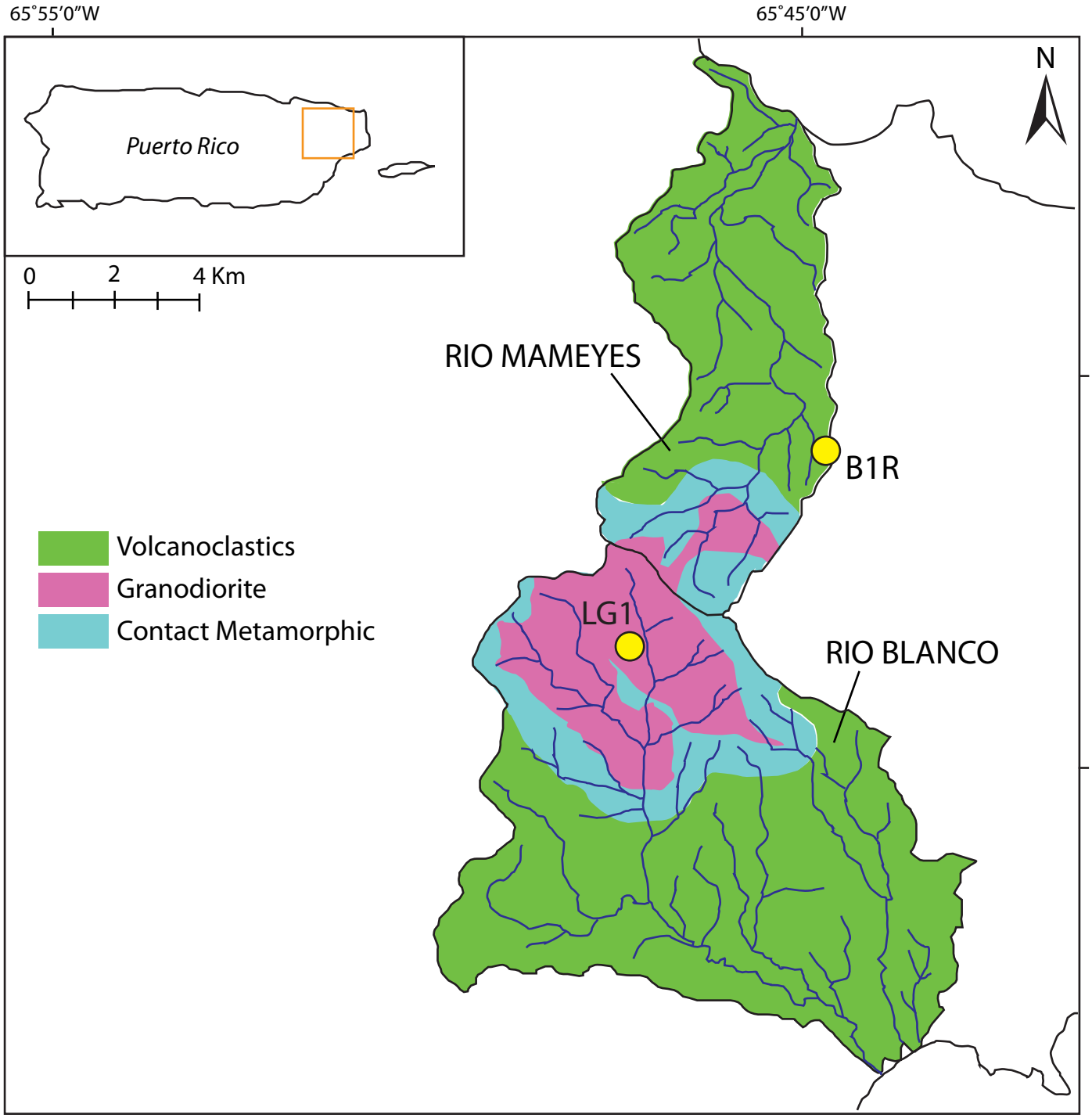

Click here to download Figure: Figure 3.pdf

Figure 3

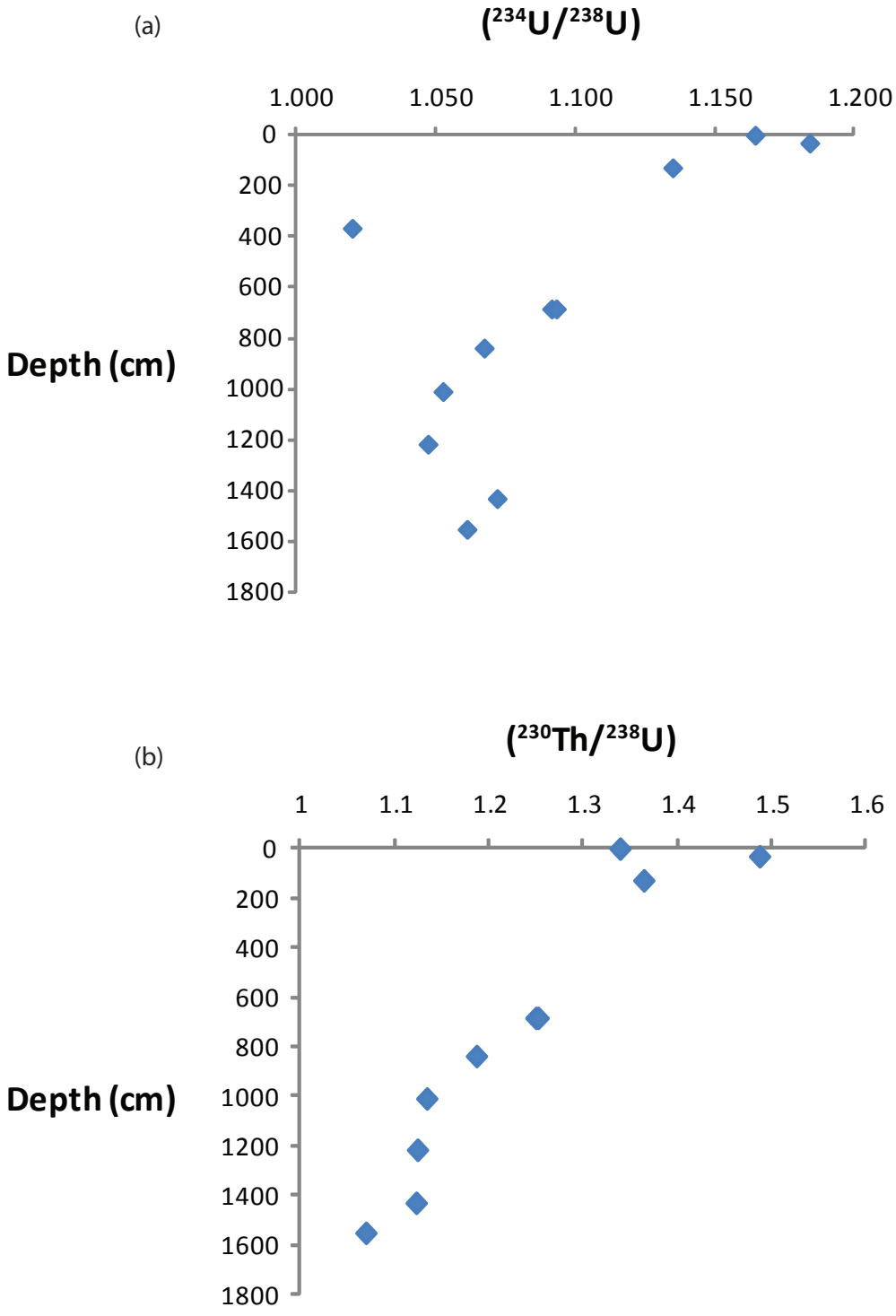

Figure 4

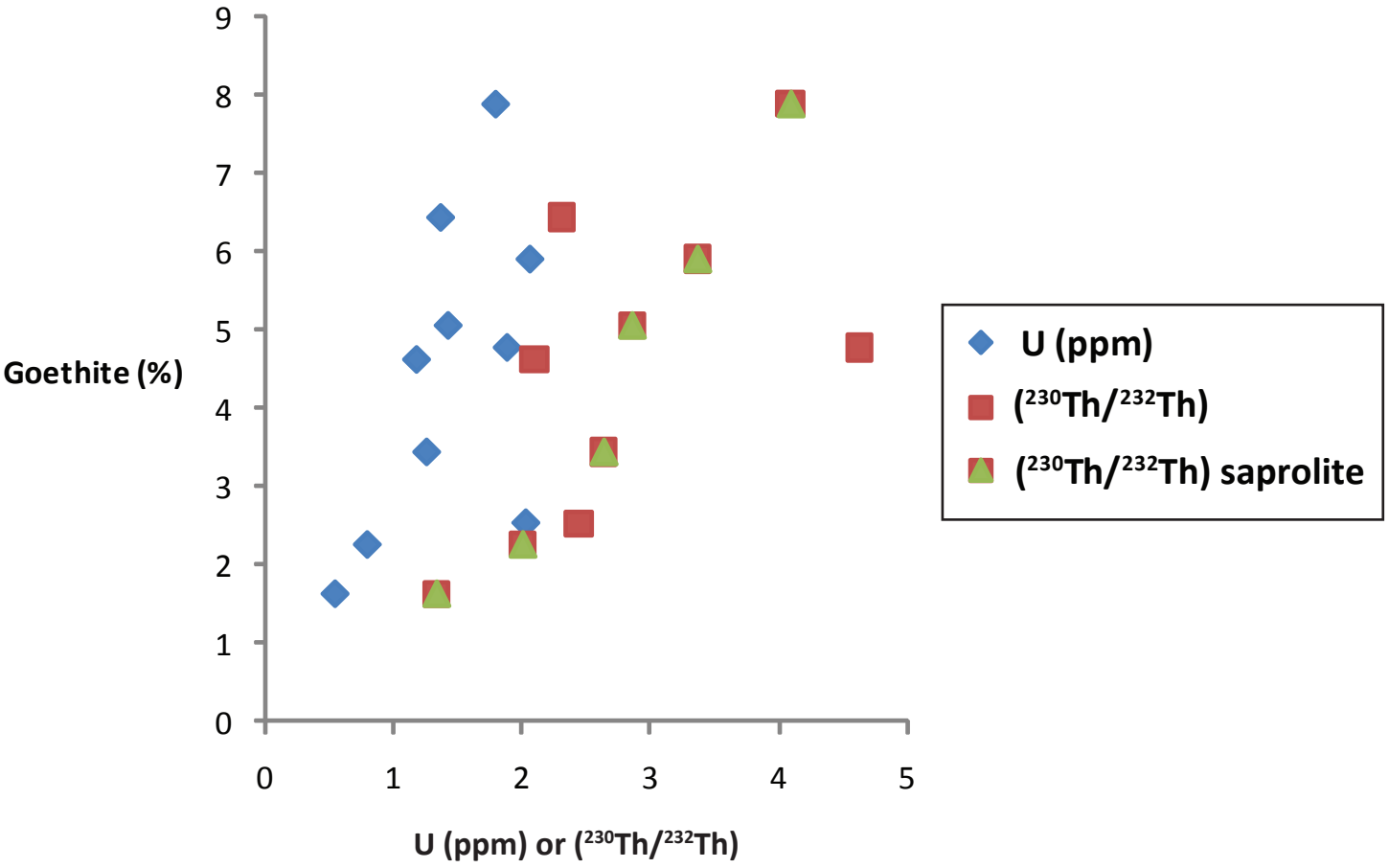

Click here to download Figure: Figure 5.pdf

Figure 5

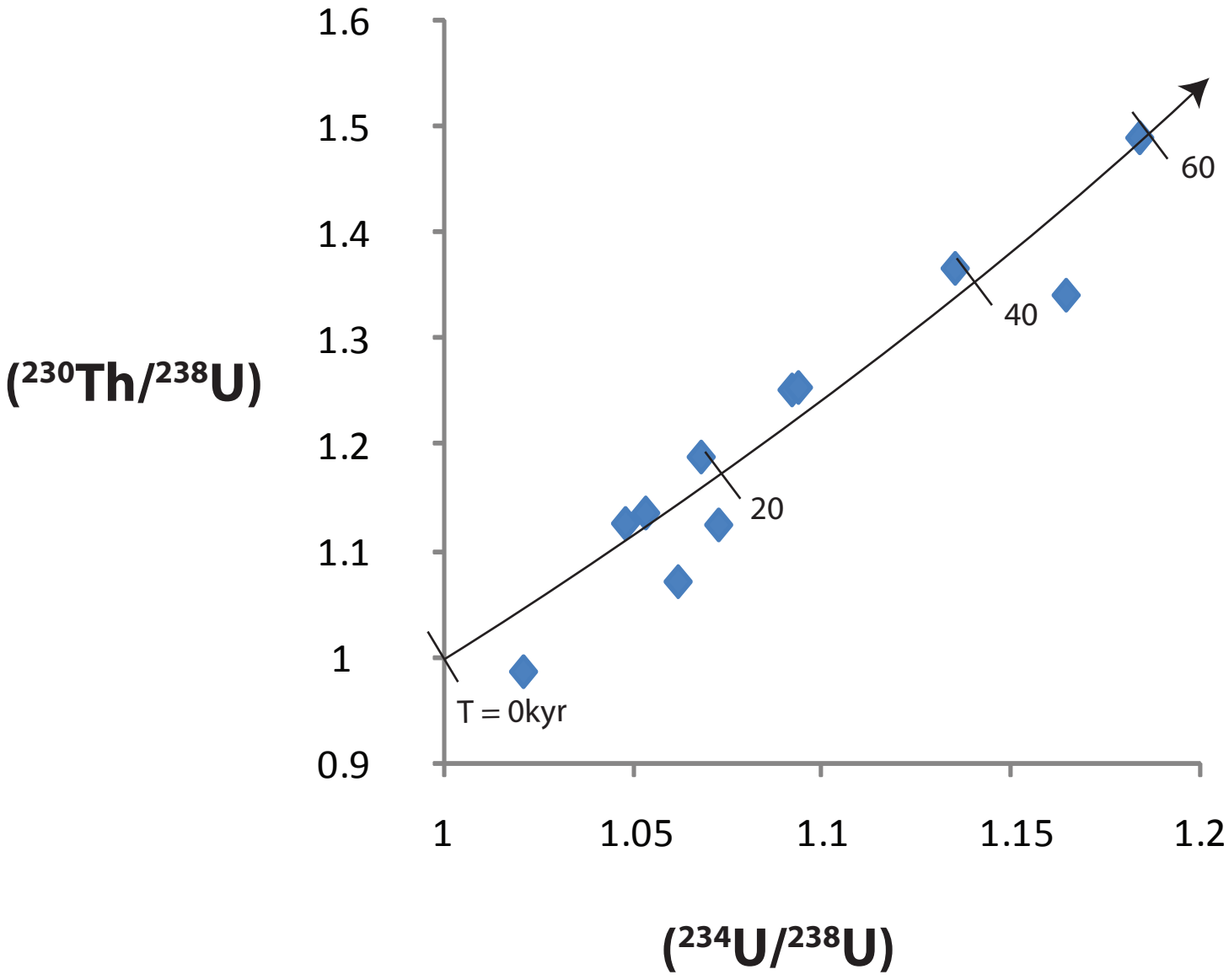

Figure 6

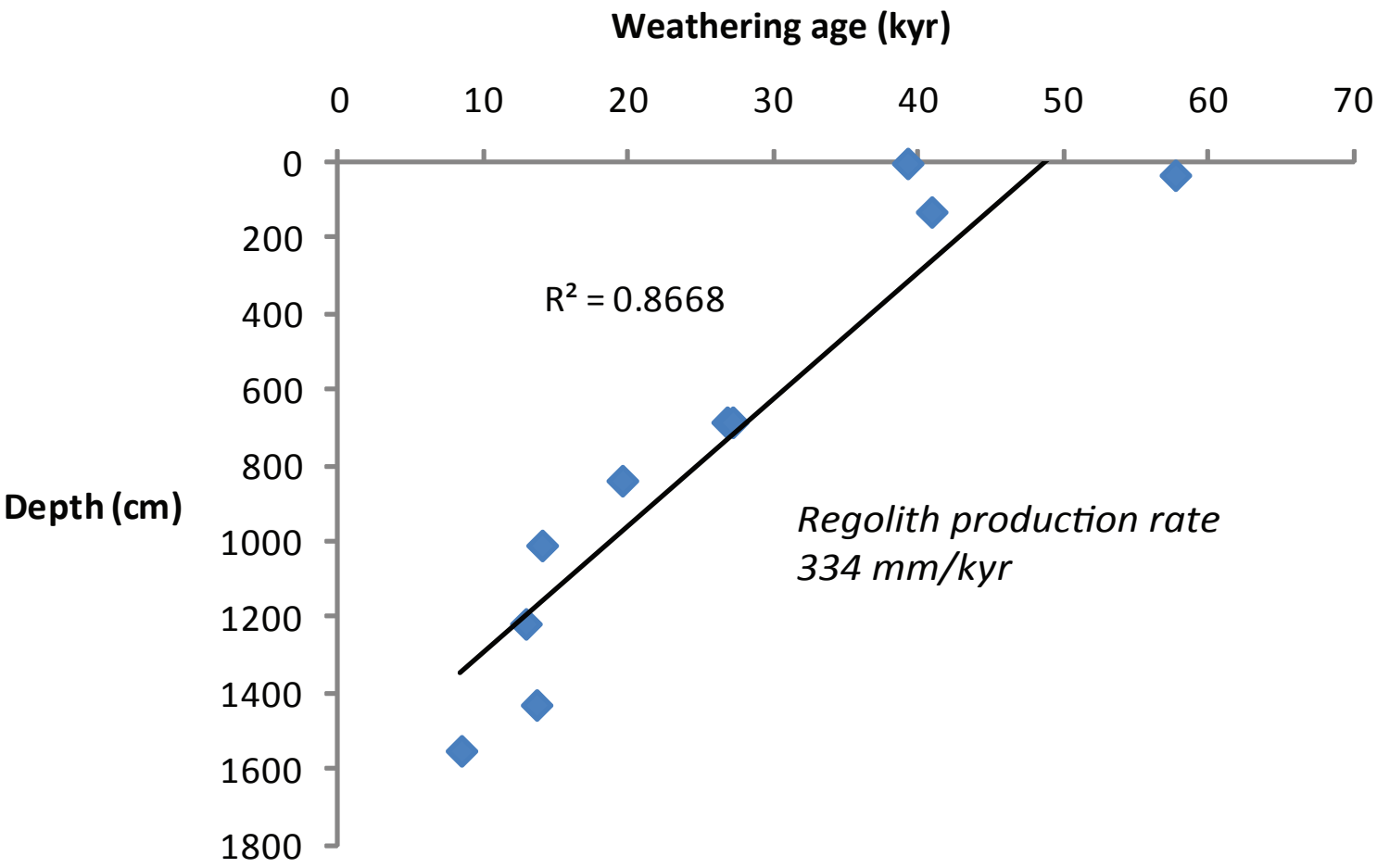

Figure 7

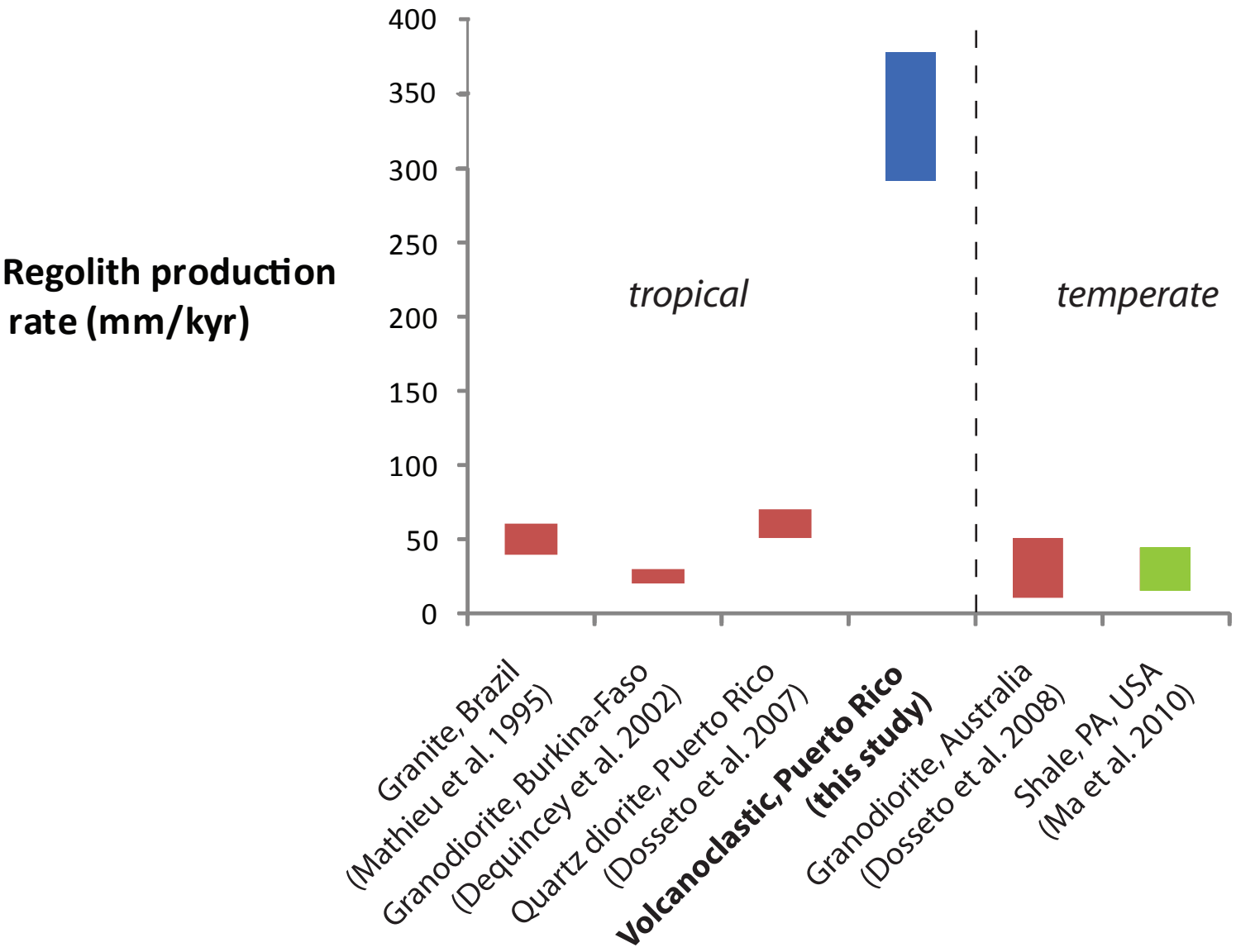

Figure 8

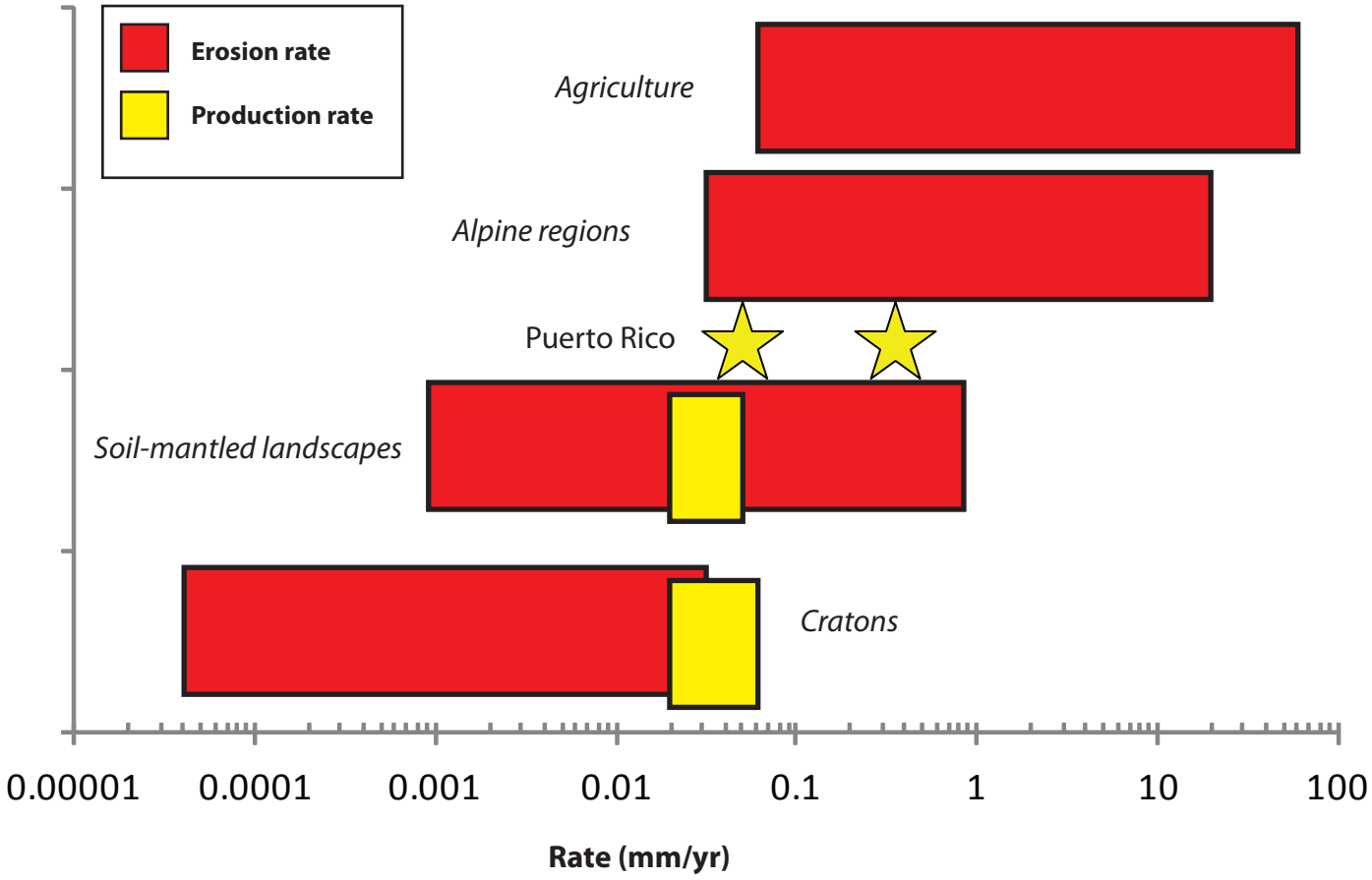

Table 1. Uranium-series isotope results

Sample name	Depth (cm)	CIA	Th (ppm)	2σ	U (ppm)	2σ	(^{234}U/^{238}U)	2σ	(^{230}Th/^{238}U)	2σ	(^{230}Th/^{232}Th)	2σ
Samples												
BIR4	4	96.7	2.292	0.003	1.184	0.001	1.165	0.002	1.340	0.004	2.097	0.003
BIR35	35	96.5	2.669	0.004	1.371	0.001	1.184	0.001	1.488	0.005	2.315	0.004
BIR132	132	96.5	1.686	0.001	1.888	0.003	1.135	0.002	1.365	0.005	4.628	0.009
BIR370	370	88.8	2.486	0.002	2.032	0.002	1.021	0.002	0.985	0.004	2.441	0.005
BIR687-1	687	95.4	1.561	0.002	0.552	0.000	1.092	0.002	1.250	0.006	1.335	0.004
BIR687-2	687		1.465	0.002	0.511	0.001	1.094	0.002	1.253	0.007	1.319	0.006
BIR841	841	98.2	1.437	0.002	0.802	0.001	1.068	0.001	1.187	0.006	2.005	0.007
BIR1012	1012	98.6	1.645	0.001	1.263	0.002	1.053	0.002	1.135	0.006	2.636	0.011
BIR1219	1219	98.4	2.091	0.002	2.065	0.003	1.048	0.001	1.125	0.005	3.365	0.010
BIR1433	1433	98.0	1.702	0.003	1.429	0.002	1.072	0.001	1.123	0.008	2.856	0.017
BIR1554	1554	96.5	1.426	0.001	1.798	0.002	1.062	0.002	1.070	0.004	4.091	0.010
parent rock Bisley	n/a	67.9 ±9.6	1.044	0.001	0.747	0.001	0.993	0.002	0.814	0.003	1.754	0.005
Rock standard												
BCR-2 (n=4)			5.63	0.03	1.61	0.02	0.991	0.006	0.999	0.007	0.868	0.003

Errors for samples are internal analytical uncertainties given at the 2σ level. The error on the CIA (Chemical Index of Alteration) value of the parent rock is 1 standard deviation of 3 replicate analyses. Errors for the rock standard BCR-2 is 2xstandard error determined from 4 replicate measurements.

Table 2. Criteria of selection of geochemical parameters (Chemical Index of Alteration (CIA) and U-series activity ratios) for the presented model

	CIA	(^{230}Th/^{232}Th)	(^{234}U/^{238}U)	(^{230}Th/^{238}U)
Sensitive to bedrock heterogeneity (incl. Hydrothermal processes)	Yes	Yes	No	No
Sensitive to the selective dissolution of minerals	Yes	Yes	No	No
Correlates with goethite content	No	Yes	No	No
Good index of weathering even in extensively weathered profiles	No	Yes	Yes	Yes
Used in the model	***No***	***No***	***Yes***	***Yes***

Table 3. Results from the nuclide loss-gain model

	Model 1 11 samples solved. Initial conditions = secular equilibrium	Model 2 10 samples solved. Initial conditions = secular equilibrium	Model 3 11 samples solved. Initial conditions = measured bedrock
k_{238} (yr^{-1})	$0.948 \pm 0.009 \times 10^{-5}$	$1.05 \pm 0.01 \times 10^{-5}$	$1.73 \pm 0.03 \times 10^{-5}$
k_{234}/k_{238}	1.09 ± 0.01	1.07 ± 0.1	1.40 ± 0.02
k_{230} (yr^{-1})	$5.01 \pm 0.8 \times 10^{-18}$	$5.57 \pm 0.8 \times 10^{-18}$	$18 \pm 2 \times 10^{-18}$
f_{238} (yr^{-1})	$0.93 \pm 0.02 \times 10^{-5}$	$1.16 \pm 0.04 \times 10^{-5}$	$0.40 \pm 0.01 \times 10^{-5}$
f_{234}/f_{238}	1.58 ± 0.02	1.57 ± 0.02	3.10 ± 0.06
f_{230} (yr^{-1})	$1.0 \pm 0.2 \times 10^{-5}$	$1.4 \pm 0.2 \times 10^{-5}$	$0.021 \pm 0.003 \times 10^{-5}$
Weathering age (kyr)			
BIR4	39.3 ± 0.3	29.9 ± 0.2	43.0 ± 0.4
BIR35	57.8 ± 0.5	43.6 ± 0.3	53.7 ± 0.5
BIR132	40.9 ± 0.3	31.1 ± 0.3	43.9 ± 0.4
BIR370	0.106 ± 0.003	n/a	14.3 ± 0.1
BIR687-1	26.8 ± 0.2	20.5 ± 0.1	34.8 ± 0.3
BIR687-2	27.2 ± 0.2	20.8 ± 0.1	35.1 ± 0.3
BIR841	19.6 ± 0.2	15.0 ± 0.1	29.8 ± 0.2
BIR1012	14.0 ± 0.1	10.7 ± 0.08	25.8 ± 0.2
BIR1219	12.9 ± 0.1	9.87 ± 0.07	25.0 ± 0.2
BIR1433	13.6 ± 0.1	10.43 ± 0.07	25.4 ± 0.2
BIR1554	8.4 ± 0.1	6.46 ± 0.05	21.3 ± 0.2
Regolith production rate (mm/kyr)	334 ± 46	443 ± 61	514 ± 63

Where 11 samples were solved, this included replicate analyses of sample BIR687. Where 10 samples were, we left out sample BIR370, which shows evidences of little weathering and probably represents a corestone (see text for details). All errors are 2 standard errors, except for the regolith production rate where the error reported is 1 standard error.

Click here to download Supplementary material for on-line publication only: Supplementary Table 1.doc

Click here to download Supplementary material for on-line publication only: Supplementary Table 2.doc

Click here to download Supplementary material for on-line publication only: Sup Fig 1.pdf

Click here to download Supplementary material for on-line publication only: Sup Fig 2.pdf